Temperature and strain SAW/BAW sensors on metallic substrates with RFID capability

Prince Mengue, Baptiste Paulmier, Sami Hage-Ali, Cyril Noirel, Marc Poncot, Cécile Floer, Hamid M'jahed, Alexander Shvetsov, Sergei Zhgoon, Pascal Nicolay, et al.

Temperature and Strain SAW/BAW Sensors on Metallic Substrates with RFID Capability

P. Mengue[1*], Baptiste Paulmier[1], S. Hage-Ali[1], Cyril Noirel[1], Marc Poncot[1], Cécile Floer[1], Hamid M'Jahed[1], Alexander Shvetsov[2], Sergei Zhgoon[2], Pascal Nicolay[3] and O. Elmazria[1]

[1]Université de Lorraine, CNRS, IJL, F-54000 Nancy, France
[2]National Research University, Moscow Power Engineering Institute, 14 Krasnokazarmennaja, 111250 Moscow, Russia
[3]Carinthia University of Applied Sciences, Europastraße 4, 9524 Villach, Austria

E-mail : prince-warol.mengue-m-owono@univ-lorraine.fr , sami.hage-ali@univ-lorraine.fr , omar.elmazria@univ-lorraine.fr

Received xxxxxx
Accepted for publication xxxxxx
Published xxxxxx

Abstract

Surface acoustic wave (SAW) strain sensors require an adhesive - typically a glue - for the mounting on the part under measurement. This comes with strain-transfer, reproducibility and aging issues. In this paper, we propose a novel glue-less solution where the SAW sensor is directly fabricated onto the surface of interest, here a metallic substrate. Here, we study the layered structure ZnO/Ti numerically and experimentally, with ZnO as the piezoelectric layer and titanium as the substrate. In this structure, both BAW (Bulk Acoustic Waves) and SAW can propagate, and we used both of them to monitor temperature variations up to 300°C and strain levels up to 1800 με. Moreover, reflective delay line (R-DL) designs were used, to provide the future users with RFID functionalities. In order to overcome the limitations due to the relatively low electromechanical coupling coefficient of ZnO/Ti, a specific R-DL layout with connected inter-digital transducers (IDTs) was used. The obtained experimental results confirm that the proposed glue-less R-DL structure is a promising solution for the independent evaluation of temperature and strain, with identification.

Keywords: Strain, temperature, SAW sensor, BAW sensor, glue-less strain sensor, radio frequency identification (RFID), connected IDTs.

1. Introduction

THIS paper is an extended version of the conference paper [1] presented at the 2021 Joint Conference of the IEEE sensors virtual conference.

Since the 1940s [2], radio frequency identification (RFID) technology has continued to evolve. It enables the identification [3] and the traceability of products and people thanks to tags that reflect signals in the form of radio waves over long distances. Whether in passive, semi-passive or active configuration, it offers a wide range of advantages that have made it a very attractive technology.

The most commonly used RFID systems are based on the use of integrated circuits (IC). They are used in various applications, such as asset management, inventory management, access control, item tracking, etc. However, the need of battery for an IC makes it less attractive for applications in difficult and/or harsh environment.

The SAW RFID technology [4] is therefore very interesting, as it opens up many possibilities for such applications.

Fig.1 summarize the generation of the RFID capability in the SAW devices. Indeed, the radio frequency (RF) interrogation is sent to the chip via the antenna. The IDTs on the sensor convert the RF pulses to the surface acoustic wave and conversely the reflected signal (R-DL) to RF pulses. The series of generated echoes corresponds to a bar code given by the position of the electrodes on the piezoelectric material. It is then possible to uniquely identify the R-DL, which is now an RFID R-DL.

SAW RFID tags also have the advantage of being very sensitive to temperature, but also in some extent to strain, magnetic field, vibration and other parameters [5–10]. It is therefore possible to use SAW RFID tags to measure various parameters in extreme environments. These devices therefore have the advantages of being fully passive (i.e. no embedded electronics, no embedded battery), robust and small. This is why they are often a very interesting solution for applications

in extreme conditions, including for Structural Health Monitoring applications.

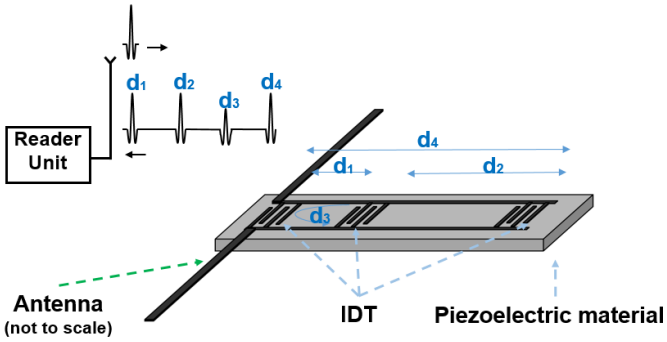

Fig. 1. Principle of wireless RFID SAW sensor interrogation

For strain measurement applications, SAW devices must in most of the cases be mounted to the part under test using adhesives (e.g. a glue). The gluing of SAW sensors must be thoroughly performed. The adhesive must be well chosen, and several critical process parameters must be accurately defined (glue thickness, annealing and curing time, and surface treatments). In addition to being a very delicate step, the use of adhesives leads to imperfect strain transfer between the part and the sensor [11], and stress relaxation/ageing of the glue can lead to measurement errors over time. Creep and hysteresis can also occur [11,12]. The heating of the adhesives during low/high temperature cycles can also cause hardness variations or early degradation of the bonding layer [12]. In some cases, the use of adhesives can also lead to the detachment of the devices [13,14].

Here, we use a glue-less solution with SAW sensors directly integrated onto the metallic part to be monitored [15]. Two strategies can be considered:

1- make the sensors directly on the part or equipment to be monitored. This solution is only compatible with small/planar pieces.

2- make the sensors on a small metal substrate and then fix the latter on the equipment to be monitored, this mounting can be done by welding or screwing which is impossible to do with a standard piezoelectric substrate.

The aim of this work is to show the feasibility of fabricating such a sensor on a metallic substrate. The latter consists of a ZnO/Ti structure, on which a R-DL structure, allowing a device identification, has been patterned. A design with connected IDTs [16] (Fig. 2) has been selected, as it generates higher amplitude peaks in comparison to standard designs. It is therefore a well-suited design for structures with moderate electromechanical coupling.

In this paper, we provide a detailed study of this sensor, with an impedance analysis in the frequency and time domain, as well as temperature, bending and tensile testing.

2. Design, Materials and Methods

The SAW device consists of a delay line with several electrically connected IDTs. Thus, most of the peaks observed in the time domain signal result from the direct transmission between connected IDTs and not reflections like in a traditional R-DL. A detailed study of this design on lithium niobate and langasite is given in [16].

Fig. 2 shows the configuration used for the ZnO/Ti devices. Here, IDTs are electrically connected and the gaps between the nearest edges of neighboring IDTs are 120λ and 180λ, respectively.

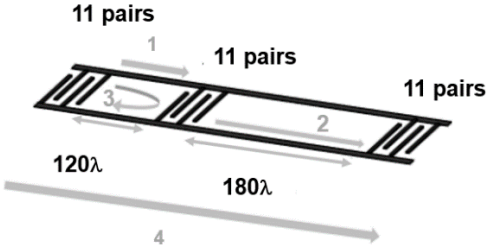

Fig. 2. RFID tag made with three electrically connected IDTs

The wavelength λ is 9.2 µm, the aperture (IDT width) is 1000 µm and metallization ratio is 50%.

In the following part, the ZnO/titanium (Fig. 3-a) structure is studied. Titanium alloy was chosen as the substrate due to its multiple advantages: it is widely used in the industry, it is lightweight and corrosion resistant. ZnO was preferred over AlN, as it is easier to deposit and presents a higher electromechanical coupling factor ($K^2 \geq 1\%$) [17,18], which is an advantage for RFID tag applications. Besides, the lower sound velocity in ZnO makes it easier to create structures without SAW energy leakage from the surface into the bulk and in the future acoustically isolated elastic waves like WLAW or ILAW[19,20]. ZnO also has a larger strain limit (1800µε at least, [15]) than AlN, which is reported to be limited to 400 µε [21].

The experimental realization of the structure was performed by depositing a 12 µm thick piezoelectric layer of ZnO on the previously mirror polished surface of a 0.5 mm thick titanium piece. RF magnetron sputtering method was used and process parameter are summarized in Table I [20] . The deposition of 12 µm of ZnO was achieved with three successive deposition steps and without removing the sample from the deposition chamber. A delay of 5 hours between two successive steps has been respected. The fabrication of the IDTs started with the deposition of a 150nm-thick aluminum film, followed by standard photolithography and etching steps. A sample fabricated device is shown in Fig. 3-b.

The modelling of the devices was performed using the following methodology: COM parameters were extracted from the Comsol Multiphysics 3D FEM computation of harmonic admittance of an elementary cell with periodic conditions. The COM parameters included in Table II were then used to calculate the device responses, using the P-Matrix method.

TABLE I
SUMMARY OF ZNO SPUTTERING PARAMETERS

Target	ZnO (Ø 4-inch)
Gases	8 sccm O_2
	8 sccm Ar
Temperature	170°C
Target power	150 W RF

Total pressure	$3x10^{-3}$ mbar

TABLE II
COM PARAMETER OF THE ZNO/TI STRUCTURE SIMULATION

Velocity	2538 m/s
Free surface velocity	2554 m/s
Reflectivity (Kappa)	1.74%
Normalized coupling coefficient	$12.28.10^{-5}$
Loss (dB/λ)	0.04
Normalized capacity	8.10^{-17}

The device was characterized by X-ray diffraction (XRD) to assess the quality of growth and the orientation of the ZnO thin film, using a Bruker D8-Advance diffractometer. The electrical characterizations were performed using a probe station (S-1160, Signatone) equipped with a heating plate up to 600 C (S-1060, Signatone), connected to a network analyzer (Agilent-N5230A and 5061B VNAs). The GS RF probes were fitted with a water-cooling circuit to ensure their cooling during the high temperature measurements. The evolution of the sensor response versus temperature (up to 300°C) and applied strain (up to 1800 με) was then characterized.

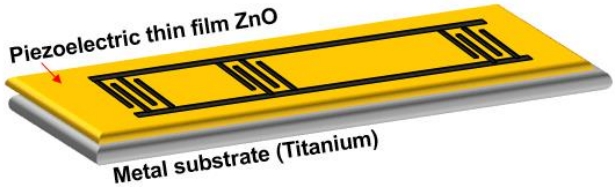

(a)

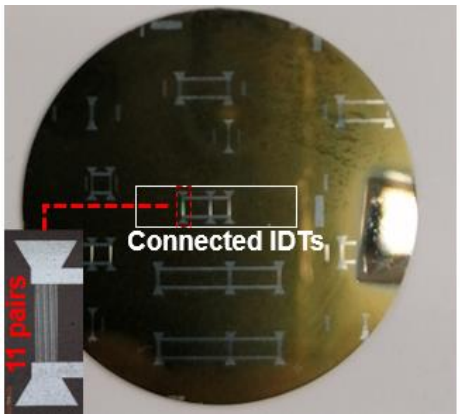

(b)

Fig. 3. (a) Schematic view of the ZnO (12µm)/Titanium(0.5mm) structure (b) Realized device

3. Results and discussion

3.1 XRD structural characterization

The XRD measurements of the ZnO layer on the titanium substrate are shown in Fig. 4. It can be seen that the deposited ZnO film has a preferential c-axis orientation. The rocking curve (FWHM) of the (002) orientation gives 1.6° and 4.85° for the 4 µm and 12 µm thicknesses of the piezoelectric ZnO deposited on titanium. The high FWHM value of the ZnO (12 µm)/Ti structure is primarily due to the scattering of the ZnO grain orientation during the growth of such a large thickness film. However, this value is sufficient for the realization of high quality SAW devices in the considered frequency range.

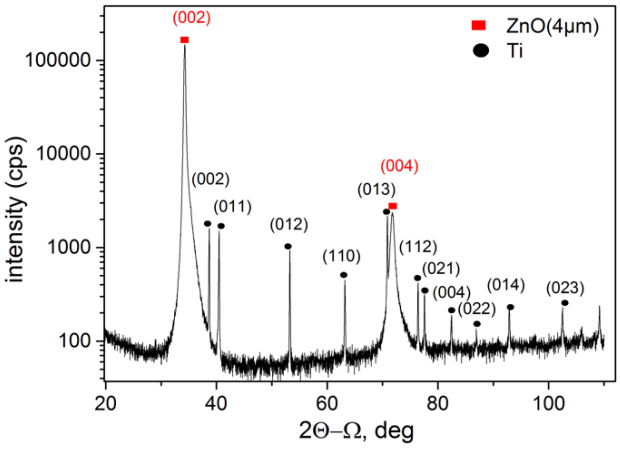

(a)

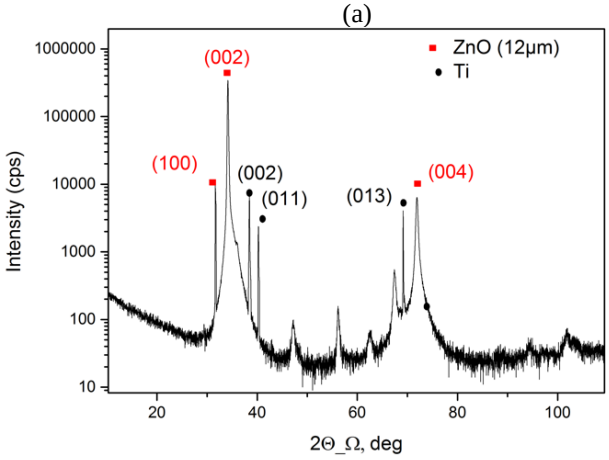

(b)

Fig. 4. XRD diagram of (a) the ZnO(4um)/titanium structure and (b) the ZnO(12um)/ Ti structure

3.2 Impedance analysis of the structure in the frequency and time domains

The measured reflection coefficient S_{11} of the ZnO/Ti structure is given in Fig. 5-a. A Rayleigh SAW [15] is observed at 280 MHz. The periodic oscillations can be attributed to longitudinal BAW (Δf_v = 5.9 MHz). The transmission of these two waves is illustrated in Fig. 5-b. The SAW is generated by the IDTs in a classical way, and propagates along the surface of the ZnO film. The BAW are mostly generated in area of the contact pads, due to the presence of the (conductive) titanium substrate under the thin ZnO layer. It is reflected by the backside of the Ti substrate. This configuration is therefore similar to H-BAR [22]. The time domain response of one device, with the different peaks due

to the different waves, is shown in Fig. 6, corresponding to a 250 to 320MHz frequency span.

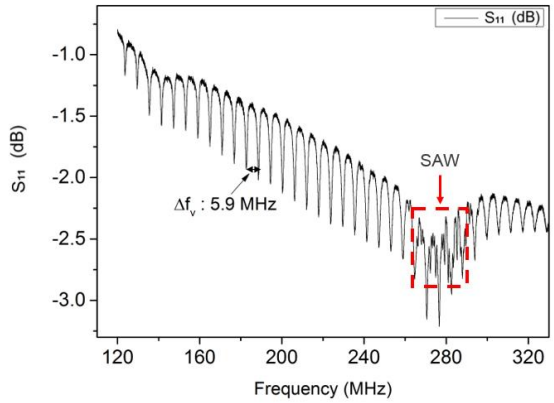

(a)

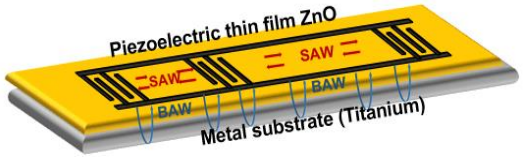

(b)

Fig. 5. (a) Experimental reflection coefficient S_{11} in the 120-320 MHz frequency range (b) illustration of the surface and bulk waves transmission in the ZnO/Ti structure

The peaks associated to BAW and SAW are labelled B_i and S_i with i={1,2,3,4}, respectively. As mentioned earlier, BAW peaks (marked by vertical red lines) and SAW peaks are very close to each other and overlap in some cases. Due to its velocity (5875m/s), the BAW is identified as a longitudinal BAW. The BAW velocity in the ZnO/Ti structure is larger than the SAW velocity (2577 m/s), which is close to the ZnO velocity (2558 m/s). This comes from the fact that the SAW energy is concentrated mainly in the ZnO layer and only in a thin region of the upper part of the Ti substrate. Indeed, the propagation depth of the SAW is mostly within one wavelength (i.e. 9.2 µm in our case) and the ZnO layer is 12 µm thick.

A very good agreement between simulation and experimental results is obtained for the main peaks, both BAW and SAW, leading to fully confirm by simulation the nature and origin of the measured peaks (see Fig. 7). From 1.25µs, a divergence between experimental and simulation results is observed. This stems from the measurement noise, which becomes, at some point, stronger than the SAW/BAW peaks.

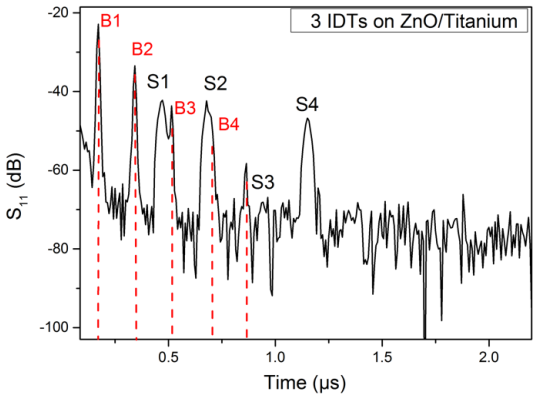

Fig. 6. Experimental reflection coefficient S_{11} in the time domain

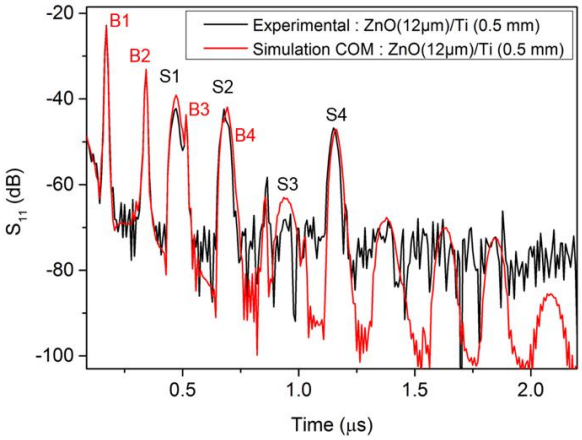

Fig. 7. Comparison of experimental and simulated reflection coefficients S_{11} in the time domain

The nature of the different peak can also be confirmed using purely experimental methods. In this case, a new device was realized on the same metallic substrate shown in Fig. 3, the IDTs were removed while the metallic contact pads were kept, in order to suppress only the SAW (see Fig. 8). Fig. 9 shows the experimental reflection coefficient S_{11} of the structure, with (black curve) and without (red curve) electrodes. It can be clearly seen that, without IDTs, the SAW peaks have completely disappeared and only the BAW peaks remain (red curve). It can also be noticed that the periodicity of the peaks corresponds to the time of a round-trip in the bilayer structure (12µm ZnO + 0.5mm Ti).

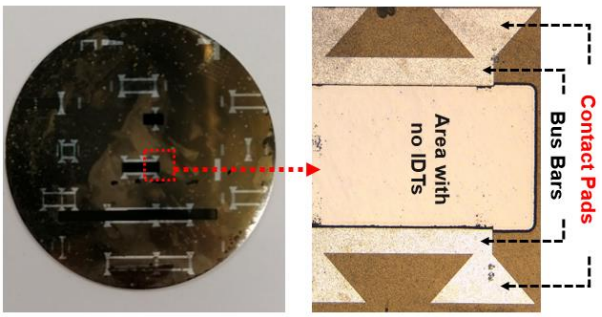

Fig. 8. Top view of the device without IDTs (left), zoom on the pads (right)

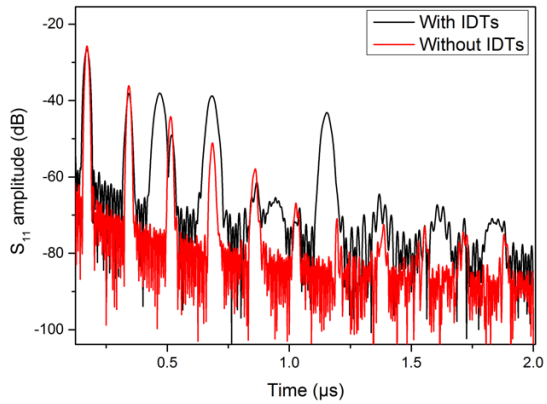

Fig. 9. Comparison of the experimental reflection coefficients S_{11} in the time domain with and without IDTs

3.3 High temperature investigation

The temperature study was performed between 25°C and 300°C. The maximum temperature has been fixed to avoid ZnO degradation [23,24]. Fig. 10-a shows the S_{11} magnitude in the time domain at various temperatures and Fig. 10-b the shows the sensitivity of each wave versus the frequency, for the S1 and B1 peaks. Since a precise peak detection in the time domain can sometimes be challenging, these frequency-dependent sensitivity curves are obtained as follows: the time domain signal is gated to encompass only the S1 or B1 peak, then analyzed in the frequency domain after Fourier transform. The frequency at a certain phase value of the reflection coefficient S_{11} is then tracked for the various temperatures. The temperature coefficient of frequency (TCF) was calculated and a good linearity can be observed for both waves. For the BAW, a very large sensitivity of -121.3 ppm/°C is obtained while it is -42.6 ppm/°C for the SAW. Experiments also show that the measured TCF values remain the same for all SAW and BAW peaks, respectively. However, peaks later in the time domain can lead to higher accuracy since the propagation way is longer.

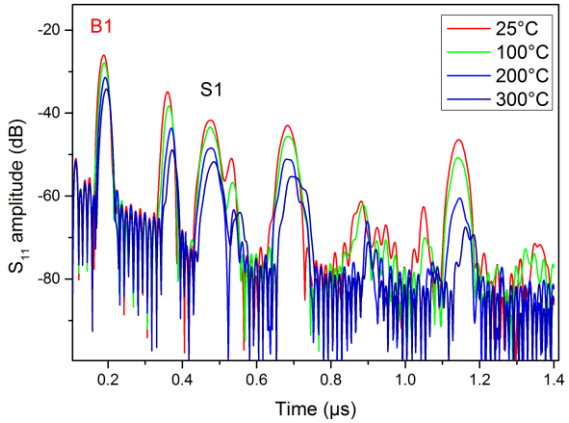

(a)

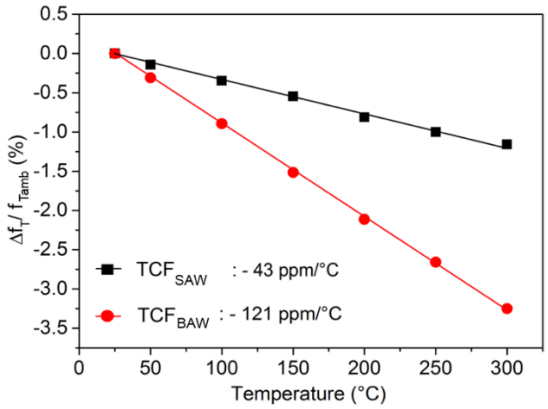

(b)

Fig. 10. (a) Experimental reflection coefficients S_{11} in time domain at various temperatures (b) relative frequency shift versus temperature for the S1 and B1 peaks

Fig. 11 shows the evolution of the S_{11} time domain amplitude versus temperature for B1 and S1 peaks. For both waves, an amplitude decrease can be seen. It is, at 300°C, around -6 dB for the bulk wave and around -15 dB for the surface wave, which can be attributed to increase of various loss mechanisms, like phonon diffusion, under high temperature. The amplitude of SAW being more adversely affected by the temperature that the amplitude of the BAW. This can be explained by the fact that SAW propagates mainly in ZnO whose acoustic propagation losses increase strongly with temperature. The BAW propagates mainly in the titanium which seems to be less affected by temperature in terms of propagation loss.

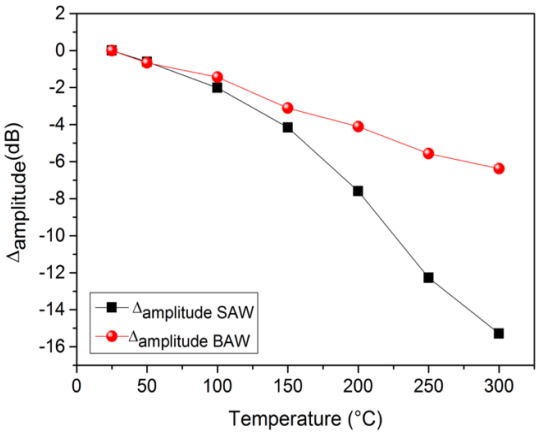

Fig. 11. Experimental evolution of the S_{11} time domain amplitude versus temperature for the B1 and S1 peaks

3.4 Influence of bending strain

Three-point bending strain tests were then performed. For these experiments, the sensor was directly integrated on a 1mm thick titanium alloy metal beam (50mm×10mm×1mm), as depicted Fig. 12a. To ensure the RF measurements, the sensor was fitted with a U. FL connector and small coaxial cable. A schematic view of the experiment is shown Fig. 12-b.

The relationship between the bending strain ε and the vertical deflection δ in this case is calculated using equations (1) and (2) [25]:

$$R^2 = (R-\delta)^2 + \left(\frac{l}{2}\right)^2, \qquad (1)$$

$$\varepsilon = \frac{(T/2)}{R}, \qquad (2)$$

where R is the radius of curvature, l is the distance between the supporting points, and T is the total thickness of the device (substrate and piezoelectric thin film).

Fig. 13 shows the frequency variation versus strain of the S1 and B1 peaks, when the bending varies from 0 με to 1800 με. Measurements were carried out at room temperature (25°C). A good linearity for both waves can be seen. The SAW exhibits a high sensitivity to bending (2.2 ppm/με). The achieved SAW sensitivity exceeds the sensitivities of conventional SAW sensors based on various piezoelectric single crystals substrates using polymeric adhesives (0.83 ppm/με in [26], 1 ppm/με in [27], 1.8 ppm/με [28]), or ceramic bonding agents (1.6 ppm/με in [29]). It also exceeds the sensitivity obtained with AlN integrated on TC4 alloy (1.6 ppm/με in [21])

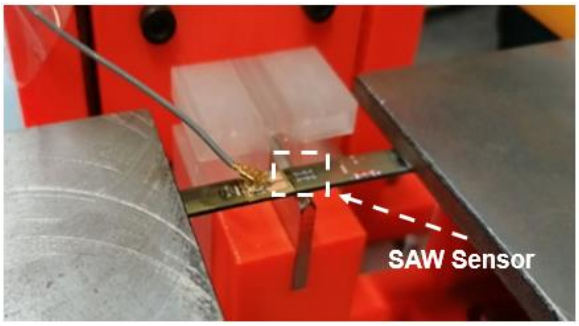

(a)

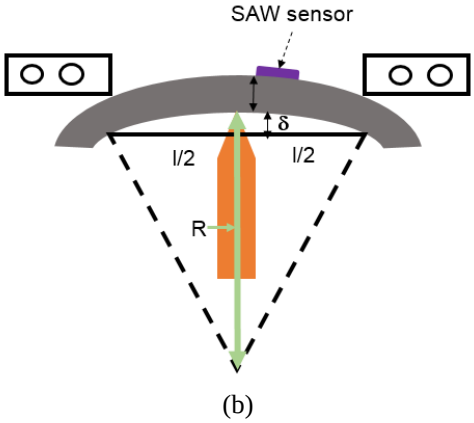

(b)

Fig. 12. (a) Experimental 3 point bending of a beam with an integrated sensor (b) illustration of the three-point bending test (adapted from [25])

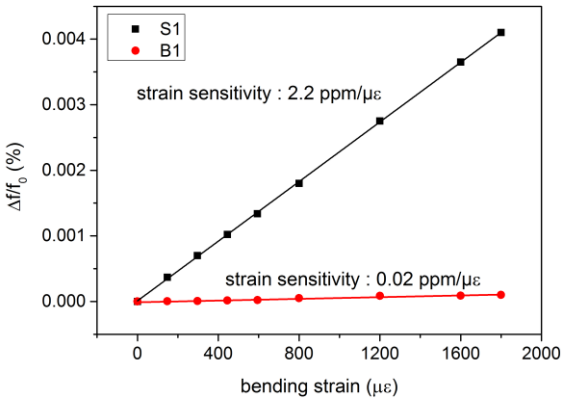

Fig. 13. Relative frequency shift versus strain applied to the metallic beam. Surface wave (black curve) and bulk wave (red curve)

On the other hand, the longitudinal BAW is almost insensitive to the bending (0.02 ppm/με). This can be explained by the facts that the thickness of ZnO/Ti remains approximately the same with bending, but also that the stresses on top and bottom are opposite, so the changes of velocity in these areas are approximately cancelling each other.

Interestingly, for practical sensing applications, we can note from sections 3.3 and 3.4 that the BAW is almost insensitive to bending and highly sensitive to the temperature, while the SAW is highly sensitive to the bending and sensitive to the temperature. Hence, the proposed structure constitutes a sensor that allows for an independent measurement of both parameters during bending: the BAW is used for the absolute temperature sensing, and for the temperature compensation of the SAW strain measurement.

3.5 Tensile testing

The structure has also been studied under tensile testing. Such an experiment generates tensile strain along the tensile axis, but also compression in the perpendicular directions. In our case, tensile strain was applied up to 900 με. Fig. 14 shows the experimental setup with the micro tensile test machine (compression-tension). The control unit allows to specify the displacement type (tension or compression) and the applied force. Different types of supports and jaws are available to adapt the machine to the needs of the desired experiment. The strain value was determined by the ratio between the length of the deformed sample and its length without strain [30]. The experimental set-up is also equipped with a resistive heating support that can reach up to 100°C. Associated thermocouple sensors are used to control the temperature of the SAW device during experiments.

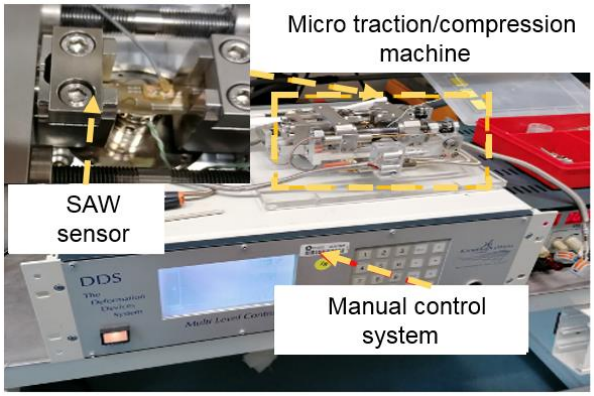

Fig. 14. Tensile test setup

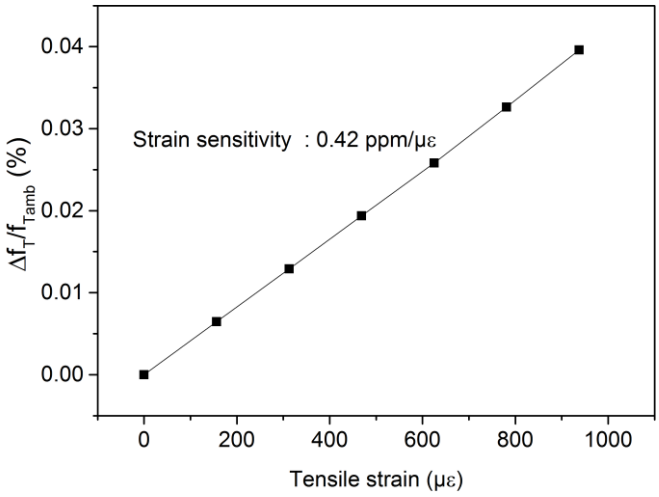

Fig. 15. Relative frequency shift of the S1 peak versus tensile stain

Experiments were first performed at room temperature (25°C). Fig. 15 shows the relative frequency variation versus tensile strain observed for the SAW S1 peak. A good linearity is obtained with a sensitivity of 0.42 ppm/με.

Based on the strain experiments (bending and tensile tests), structure shows a higher sensitivity in the three-point bending than in the tensile test. This is due to the fact that the stress-related contributions to the elastic constants impact the Rayleigh wave differently for each type of deformation.

3.6 Investigation of the temperature influence on the tensile testing

Tensile tests were performed on the structure up to 80°C, using the same setup as previously. The tensile strain was applied up to 900 με. Results for the S1 peak are given in Fig. 16. Once again, a very good linearity is observed, at different temperatures. Also, the sensitivity decreases when the temperature increases. The sensitivity decreases from 0.42 ppm/με at 20°C to 0.15 ppm/με at 80°C, which implies the need of a temperature compensation. The dependence between the effects of temperature and bending stresses is mainly due to the internal behavior of the physical and in particular elastic properties of the materials constituting the sensors. This dependence has also been observed on previous works using other materials ([11],[31]).

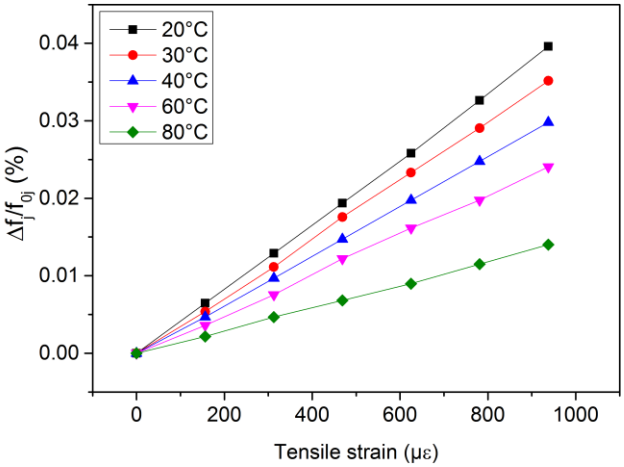

Fig. 16. Relative frequency shift $(f_j-f_{0j})/f_{0j}$ of the S1 peak versus tensile strain at various temperatures. f_{0j} are the reference frequencies at 0 strain for j={20°C,30°C,40°C,60°C,80°C}

4. Conclusion

In this study, ZnO/Ti acoustic wave sensors with RFID capability were fabricated and characterized. The connected IDTs configuration was used to improve the signal quality. The deposition of ZnO on metal opens up very interesting application possibilities, where the use of an adhesive is no longer necessary, for the direct integration of sensors on test bodies, especially for strain measurements.

It is found that this structure allows the generation of two types of waves, surface acoustic waves and bulk acoustic waves.

The structure was tested at high temperature up to 300°C. The results show a sensitivity of -121 ppm/°C and -43 ppm/°C for the BAW and the SAW, respectively. The SAW was found to be highly sensitive to the bending (2.2 ppm/με), while the BAW is almost insensitive to this type of deformation. This behavior is very advantageous since the BAW can serve as a temperature reference for the temperature compensation of SAW strain measurement.

Finally, the structure was subjected to tensile strain (up to 900 με), under temperatures up to 80°C. The sensitivity to strain decreased from 0.42 ppm/με (at room temperature) to 0.15 ppm/με (at 80°C).

As a conclusion, the proposed directly integrated, glue-less SAW/BAW sensor has a great potential for the monitoring of temperature and strain on metal parts, which are crucial for structural health monitoring applications.

Acknowledgements

This work was supported by Campus France Gabon, the French PIA project 'Lorraine University of Excellence' (ANR-15-IDEX-04 LUE) and the CAPMAT project ('FEDER-FSE Lorraine et Massif Vosges 2014–2020' and ICEEL). The

MiNaLor cleanroom platform is partially supported by FEDER and Grand Est Region through the RaNGE project.

The authors would like to thank Laurent Badie, Gwladys Lengaigne and Carlos Rojas from MiNaLor cleanroom at Institut Jean Lamour for their help in the fabrication.

References

[1] Mengue P, Paulmier B, Hage-Ali S, Floer C, M'Jahed H, Shvetsov A, Zhgoon S and Elmazria O 2021 SAW-RFID temperature and strain sensors on metallic substrates *2021 IEEE Sensors* 2021 IEEE Sensors pp 1–4

[2] Stockman H 1948 Communication by Means of Reflected Power *Proc. IRE* **36** 1196–204

[3] Rieback M R, Crispo B and Tanenbaum A S 2006 The evolution of RFID security *IEEE Pervasive Comput.* **5** 62–9

[4] Campbell C K 1998 *Surface Acoustic Wave Devices for Mobile and Wireless Communications, Four-Volume Set* (San Diego: Academic Press)

[5] Binder A, Bruckner G, Schobernig N and Schmitt D 2013 Wireless Surface Acoustic Wave Pressure and Temperature Sensor With Unique Identification Based on LiNbO3 *IEEE Sens. J.* **13** 1801–5

[6] Scherr H, Scholl G, Seifert F and Weigel R 1996 Quartz pressure sensor based on SAW reflective delay line *1996 IEEE Ultrasonics Symposium. Proceedings* 1996 IEEE Ultrasonics Symposium. Proceedings vol 1 pp 347–50 vol.1

[7] Fachberger R, Bruckner G, Hauser R and Reindl L 2006 Wireless SAW based high-temperature measurement systems *2006 IEEE International Frequency Control Symposium and Exposition* 2006 IEEE International Frequency Control Symposium and Exposition pp 358–67

[8] Mishra H, Streque J, Hehn M, Mengue P, M'Jahed H, Lacour D, Dumesnil K, Petit-Watelot S, Zhgoon S, Polewczyk V, Mazzamurro A, Talbi A, Hage-Ali S and Elmazria O 2020 Temperature compensated magnetic field sensor based on love waves *Smart Mater. Struct.* **29** 045036

[9] Yang Y, Mishra H, Mengue P, Hage-Ali S, Petit-Watelot S, Lacour D, Hehn M, M'Jahed H, Han T and Elmazria O 2020 Enhanced Performance Love Wave Magnetic Field Sensors With Temperature Compensation *IEEE Sens. J.* **20** 11292–301

[10] Yang Y, Mengue P, Mishra H, Floer C, Hage-Ali S, Petit-Watelot S, Lacour D, Hehn M, Han T and Elmazria O 2022 Wireless Multifunctional Surface Acoustic Wave Sensor for Magnetic Field and Temperature Monitoring *Adv. Mater. Technol.* **7** 2100860

[11] Kalinin V 2014 Modelling of hysteresis and creep in SAW strain sensors *2014 IEEE International Frequency Control Symposium (FCS)* 2014 IEEE International Frequency Control Symposium (FCS) pp 1–4

[12] Beckley J, Kalinin V, Lee M and Voliansky K 2002 Non-contact torque sensors based on SAW resonators *Proceedings of the 2002 IEEE International Frequency Control Symposium and PDA Exhibition (Cat. No.02CH37234)* pp 202–13

[13] Maskay A, Hummels D M and Pereira da Cunha M 2018 SAWR dynamic strain sensor detection mechanism for high-temperature harsh-environment wireless applications *Measurement* **126** 318–21

[14] Oishi M, Hamashima H and Kondoh J 2016 Measurement of cantilever vibration using impedance-loaded surface acoustic wave sensor *Jpn. J. Appl. Phys.* **55** 07KD06

[15] Mengue P, Hage-Ali S, Zhgoon S, Paulmier B, Floer C, Bartoli F and Elmazria O 2021 Direct integration of SAW resonators on industrial metal for structural health monitoring applications *Smart Mater. Struct.* **30** 125009

[16] Floer C, Hage-Ali S, Nicolay P, Chambon H, Zhgoon S, Shvetsov A, Streque J, M'Jahed H and Elmazria O 2020 SAW RFID Devices Using Connected IDTs as an Alternative to Conventional Reflectors for Harsh Environments *IEEE Trans Ultrason Ferroelectr Freq Control* **67** 1267–74

[17] Ieki H and Kadota M 1999 ZnO thin films for high frequency SAW devices *1999 IEEE Ultrasonics Symposium. Proceedings. International Symposium (Cat. No.99CH37027)* 1999 IEEE Ultrasonics Symposium. Proceedings. International Symposium (Cat. No.99CH37027) vol 1 pp 281–9 vol.1

[18] Le Brizoual L, Sarry F, Elmazria O, Alnot P, Ballandras S and Pastureaud T 2008 GHz frequency ZnO/Si SAW device *IEEE Trans. Ultrason. Ferroelectr. Freq. Control* **55** 442–50

[19] Bhattacharjee K, Shvetsov A and Zhgoon S 2007 Packageless SAW Devices with Isolated Layer Acoustic Waves (ILAW) and Waveguiding Layer Acoustic Waves (WLAW) *2007 IEEE International Frequency Control Symposium Joint with the 21st European Frequency and Time Forum* 2007 IEEE International Frequency Control Symposium Joint with the 21st European Frequency and Time Forum pp 135–40

[20] Floer C, Hage-Ali S, Zhgoon S, Moutaouekkil M, Bartoli F, Mishra H, McMurtry S, Pigeat P, Aubert T, Bou Matar O, Talbi A and Elmazria O 2018 AlN/ZnO/$LiNbO_3$ Packageless Structure as a Low-Profile Sensor for Potential On-Body Applications *IEEE Trans. Ultrason. Ferroelectr. Freq. Control* **65** 1925–32

[21] Shu L, Wang X, Li L, Yan D, Peng L, Fan L and Wu W 2019 The investigation of integrated SAW strain sensor based on AlN/TC4 structure *Sens. Actuators Phys.* **293** 14–20

[22] Baron T, Lebrasseur E, Bassignot F, Martin G, Pétrini V, Ballandras S, Baron T, Lebrasseur E, Bassignot F, Martin G, Pétrini V and Ballandras S 2013 *High-Overtone Bulk Acoustic Resonator* (IntechOpen)

[23] Khudiar A 2013 Fabrication temperature sensing by using ZnO Nanoparticles *J. THI- QAR Sci. ISSN 1991- 8690* **4** 75

[24] Saravanakumar K, Senthilkumar V, Sanjeeviraja C, Jayachandran M, Ganesan V, Koizhaiganova R B, Vasudevan T and Lee M S 2008 The influence of substrate temperature on the electrical properties of zno films prepared by the rf magnetron sputtering technique *Nano* **03** 469–76

[25] Eun K, Lee K J, Lee K K, Yang S S and Choa S-H 2016 Highly sensitive surface acoustic wave strain sensor for the measurement of tire deformation *Int. J. Precis. Eng. Manuf.* **17** 699–707

[26] Nomura T, Kosaka T, Saitoh A and Furukawa S 2006 Passive Strain Sensor using SH-SAW Reflective Delay Line *Ferroelectrics* **333** 121–9

[27] Donohoe B, Geraghty D, O'Donnell G E and Stoney R 2012 Packaging Considerations for a Surface Acoustic Wave Strain Sensor *IEEE Sens. J.* **12** 922–5

[28] Humphries J R and Malocha D C 2015 Wireless SAW Strain Sensor Using Orthogonal Frequency Coding *IEEE Sens. J.* **15** 5527–34

[29] Shu L, Peng B, Yang Z, Wang R, Deng S and Liu X 2015 High-Temperature SAW Wireless Strain Sensor with Langasite *Sensors* **15** 28531–42

[30] Shah J 1980 Strain Sensivity of Thick-Film Resistors *IEEE Trans. Compon. Hybrids Manuf. Technol.* **3** 554–64

[31] Xu H, Dong S, Xuan W, Farooq U, Huang S, Li M, Wu T, Jin H, Wang X and Luo J 2018 Flexible surface acoustic wave strain sensor based on single crystalline LiNbO3 thin film *Appl. Phys. Lett.* **112** 093502